Proc. Natl. Acad. Sci. USA
Vol. 93, pp. 7481–7485, July 1996
Biochemistry

Structure of the catalytic fragment of poly(ADP-ribose) polymerase from chicken

(DNA repair/NAD$^+$/nicotinamide analogue/X-ray crystallography/bacterial toxins)

ARMIN RUF*, JOSIANE MÉNISSIER DE MURCIA†, GILBERT M. DE MURCIA†, AND GEORG E. SCHULZ*‡

*Institut für Organische Chemie und Biochemie, Albertstrasse 21, D-79104 Freiburg im Breisgau, Germany; and †École Supérieure de Biotechnologie de Strasbourg, UPR 9003 du Centre National de la Recherche Scientifique, Cancérogenèse et Mutagenèse Moléculaire et Structurale, Boulevard Sébastien Brant, F-67400 Illkirch-Graffenstaden, France

Communicated by Takashi Sugimura, National Cancer Center, Tokyo, Japan, March 25, 1996 (received for review December 25, 1995)

ABSTRACT **The crystal structures of the catalytic fragment of chicken poly(ADP-ribose) polymerase [NAD$^+$ ADP-ribosyltransferase; NAD$^+$:poly(adenosine-diphosphate-D-ribosyl)-acceptor ADP-D-ribosyltransferase, EC 2.4.2.30] with and without a nicotinamide-analogue inhibitor have been elucidated. Because this enzyme is involved in the regulation of DNA repair, its inhibitors are of interest for cancer therapy. The inhibitor shows the nicotinamide site and also suggests the adenosine site. The enzyme is structurally related to bacterial ADP-ribosylating toxins but contains an additional α-helical domain that is suggested to relay the activation signal issued on binding to damaged DNA.**

DNA strand breaks introduced by DNA damaging agents trigger the endogenous synthesis of poly(ADP-ribose) by the enzyme poly(ADP-ribose) polymerase (PARP, NAD$^+$: ADP-ribosyltransferase; NAD$^+$:poly(adenosine-diphosphate-D-ribosyl)-acceptor ADP-D-ribosyltransferase, EC 2.4.2.30). In response to a break, PARP catalyzes the covalent attachment of ADP-ribose units from NAD$^+$ to itself (automodification) and to a limited number of nuclear DNA-binding proteins (heteromodification), thus decreasing their affinity for DNA (1, 2). The reaction is NAD$^+$ + $X \rightarrow X$-1′-ribose-5′-ADP + nicotinamide, where X is a side chain of a protein to be modified (generally a glutamate, chain initiation), or the 2′- or 3′-OH group of the ADP moiety of monomeric or polymeric ADP-ribose (chain elongation or branching), or water (hydrolysis). PARP has emerged in the last decade as a critical regulatory component of the immediate cellular response to DNA damage; in particular, it affects base excision repair (3–5). When bound to nicked DNA and activated, PARP is a homodimer of M_r 2 × 113,000. The polypeptide has a highly conserved modular organization consisting of an N-terminal DNA-binding domain (apparent M_r 46,000), a central regulating segment (apparent M_r 22,000), and a C-terminal region (apparent M_r 54,000) accommodating the catalytic center (6). The N-terminal domain acts as a DNA nick sensor, encompassing two zinc-finger motifs and a bipartite nuclear location signal. The central segment carries ADP-ribosylation sites modulating the interaction of PARP with DNA. The C-terminal region is the most strictly conserved part of the enzyme. It can be cut down to a 40-kDa C-terminal polypeptide without losing the basal catalytic activity (7). The structure of this catalytically competent 40-kDa fragment of PARP from chicken (PARP-CF, corresponding to functional region F of ref. 6) is here reported.

METHODS

The 40-kDa C-terminal catalytic fragment of PARP from chicken, PARP-CF, was expressed in insect cells (*Spodoptera frugiperda*, Sf9). PARP-CF comprises residues 654–1014. Because most of the literature refers to human PARP, we use human numbering throughout the text (subtract 3 for the respective chicken numbers in PARP-CF). PARP-CF was then purified and crystallized as described (8). Macroseeding in hanging drops yielded crystals suitable for x-ray analysis. The crystals belong to space group $P2_12_12_1$ with unit cell dimensions 59.3 × 65.0 × 96.7 Å^3 and one molecule PARP-CF in the asymmetric unit.

The structure was solved by multiple isomorphous replacement based on three heavy atom derivatives (Table 1). All data except for the inhibitor complex were collected with a multiwire area detector (model X-1000; Siemens, Karlsruhe, Germany) by using Cu K_α radiation from a rotating anode generator (model RU200B, Rigaku, Tokyo; model M18XHF, Siemens). The mercury sites were determined by difference Patterson maps, whereas iridium was located by a difference Fourier map. The heavy atom parameters were refined with program ML-PHARE (9), and phases were improved by solvent flattening and histogram matching in program DM (10). For this analysis, we took data set Native-1. The resulting electron density map was used to build a poly-alanine model consisting of numerous short fragments covering 264 of the 361 residues of PARP-CF. The model was completed by manual model building in program O (11) by using σ_A-weighted MIR maps at 2.9-Å resolution together with positional refinement in X-PLOR (12). Simulated annealing refinement (12) was continued with data set Native-2 (Table 2). The present model incorporates residues 662-1010 of PARP-CF together with 50 solvent molecules. The first eight and the last four residues of the polypeptide could not be located. Apart from other indices, the good quality of the resulting model is best demonstrated by the Ramachandran quality (14) stated in Table 2.

The x-ray diffraction data set of the enzyme/inhibitor complex was collected on an image plate (MAR Research, Hamburg, Germany) with synchrotron radiation (European Molecular Biology Laboratory outstation, Deutsches Elektronen Synchrotron, Hamburg) using a crystal produced by cocrystallization of PARP-CF with 1.8 mM of the NAD$^+$ analogue inhibitor PD128763 (see Fig. 3). The crystals were isomorphous with the native enzyme crystals. The inhibitor was clearly visible in the initial ($F_o - F_c$) electron density map at 2.4-Å resolution. The structure was refined with X-PLOR (12).

The publication costs of this article were defrayed in part by page charge payment. This article must therefore be hereby marked "*advertisement*" in accordance with 18 U.S.C. §1734 solely to indicate this fact.

Abbreviations: PARP, poly(ADP-ribose)polymerase; PARP-CF, PARP catalytic fragment (residues 655-1014, human numbering).

Data deposition: The atomic coordinates and structure factors have been deposited in the Protein Data Bank, Chemistry Department, Brookhaven National Laboratory, Upton, NY 11973 (reference 1PAW, 1PAX). This information is embargoed for 1 year (coordinates) and 1 year (structure factors) from the date of publication.

‡To whom reprint requests should be addressed. e-mail: schulz@bio5.chemie.uni-freiburg.de.

Table 1. Structure determination

		Heavy atom derivatives		
	Native-1	Na_2HgI_4	MMA*	Na_3IrCl_6
Resolution, Å	20–2.7	20–2.9	20–3.5	20–3.3
Completeness, %	83.1	75.9	80.2	78.8
R_{sym},† %	6.1	5.1	9.3	4.2
Reflections	9154	6605	3872	4493
R_{iso},‡ %	—	12.3	12.5	11.2
Site x/y/z	—	0.69/0.64/ 0.67	0.65/0.66/ 0.67	0.12/0.28/ 0.23
Phasing power	—	1.05	1.00	0.57

*MMA, methylmercury acetate.
†$R_{sym} = \Sigma_h\Sigma_i|I(h)_i - <I\ (h)>|/\Sigma_h\Sigma_i I(h)_i$.
‡$R_{iso} = 2\cdot\Sigma|F_{der} - F_{nat}|/\Sigma(F_{der}+F_{nat})$.

RESULTS AND DISCUSSION

Description of the Structure. PARP-CF is composed of two parts: a purely α-helical N-terminal domain of residues 662–784, and a C-terminal domain of residues 785-1010 bearing the putative NAD^+ binding site (Fig. 1). The N-terminal domain consists of an up-up-down-up-down-down motif of helices (Fig. 2), in which the connections B–C, E–F, and F–G are 9 to 14 residues long. The core of the C-terminal domain is formed by a five-stranded antiparallel β-sheet and a four-stranded mixed β-sheet. These two sheets are connected via a single pair of hydrogen bonds between strands c and d. Strands c and d run at an angle of 90°. The sheets are consecutive as sketched in

Table 2. Refinement and model statistics

	Native-2	Inhibitor complex
Resolution, Å	10–2.5	10–2.4
Completeness, %	93.6	99.3
R_{sym}, %	6.3	6.5
Unique reflections	12,355	14,847
No. of located atoms	2755	2767
No. of water molecules	50	70
R-factor, %	21.4	21.2
Free R-factor,* %	32.7	31.2
Overall B-factor, $Å^2$	16	24
B-factor of inhibitor, $Å^2$	—	10
rms bond length deviation, Å	0.012	0.013
rms bond angle deviation, °	1.6	1.7
rms B-factor difference†		
Along a bond, $Å^2$	1.0 (1.3)	1.1 (1.6)
Along an angle, $Å^2$	1.7 (2.2)	1.9 (2.7)
Ramachandran quality,‡ %	87	89

*The fraction of reflections was 10% (13).
†Values for main chain atoms; in parentheses, values for side chains.
‡Defined as the fraction of nonglycine nonproline residues with (φ, ψ)-angles in the "most favored regions" according to ref. 14. The only residue in a "disallowed region" is Met-746 in structure Native-2.

Fig. 2. The central β-sheets are surrounded by five α-helices, three 3_{10}-helices, and by a three- and a two-stranded β-sheet in a 37-residue excursion between the two central β-strands g and m.

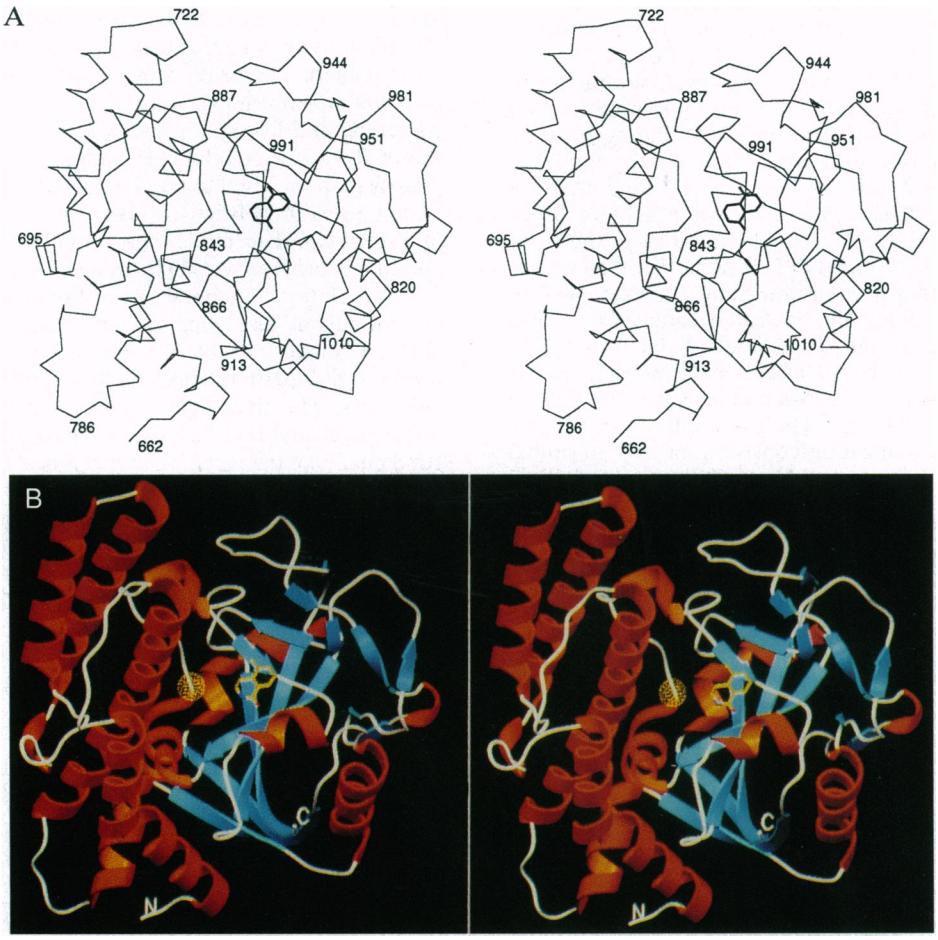

FIG. 1. Catalytic fragment of PARP-CF. (*A*) Stereoview of the C^α backbone of PARP-CF (residues 662-1010, human numbering). The crystallized polypeptide contains eight more N-terminal and four more C-terminal residues. The orientation of the inhibitor PD128763 (see Fig. 3) can be recognized by the puckered lactame ring. (*B*) Stereoview of PARP-CF as ribbon; the inhibitor PD128763 is shown in yellow. The dotted sphere represents the putative adenine binding site.

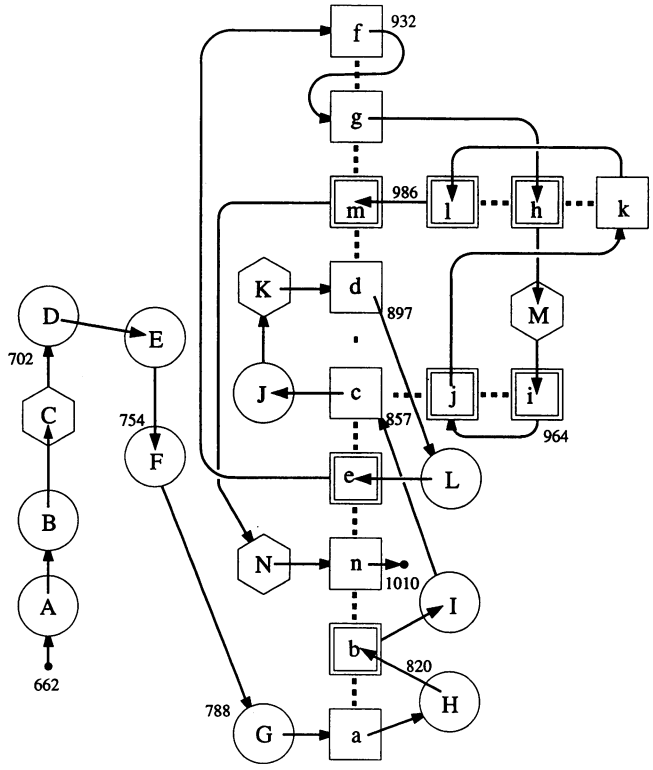

FIG. 2. Topology sketch of PARP-CF showing β-strands a–n and helices A–N. α-Helices are depicted as circles, 3_{10}-helices are hexagons, and β-strands are squares. Concentric squares indicate β-strands running into the paper plane. Some residue numbers are given. Hydrogen bonds in β-sheets are indicated by dots. β-strands c and d run at an angle of 90° and merely form two hydrogen bonds with each other. These connect residues 861 and 898.

Two very different models have been proposed for PARP-CF. One is based on weak sequence similarities with ADP-ribosylating toxins (15), and the other on sequence similarities to NAD(P)-dependent leucine and glutamate dehydrogenases (16). Both models were compatible with site-directed mutagenesis experiments hitting presumed active site residues (16, 17). Now the presented x-ray structure decides this riddle in favor of the toxins. The chain fold of PARP-CF is similar to the folds of the catalytic domains of diphtheria toxin from

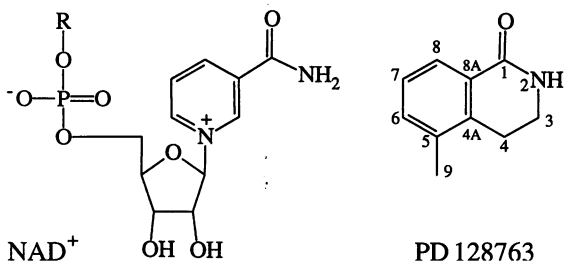

FIG. 3. Covalent structure of inhibitor PD128763 that mimics the nicotinamide moiety of NAD^+ (31).

Corynebacterium diphtheriae (18–21), exotoxin A from *Pseudomonas aeruginosa* (22, 23), heat-labile enterotoxin from *Escherichia coli* (24), pertussis toxin from *Bordetella pertussis* (25), and cholera toxin from *Vibrio cholerae* (26). It differs grossly from the Rossmann fold of a glutamate dehydrogenase (27).

Inhibitor Binding. Specific inhibitors of PARP are of particular clinical interest because they potentiate the cytotoxic effects of radiation and alkylating agents by inhibiting DNA repair (28–30). The nicotinamide analogue inhibitor PD128763 (3,4-dihydro-5-methyl-isoquinolinone; Parke–Davis/Warner–Lambert) (31) (Fig. 3) could be cocrystallized with PARP-CF and structurally analyzed at 2.4-Å resolution. The model of the complex is of good quality (Table 2).

The inhibitor is bound to PARP-CF by two hydrogen bonds from its lactame group to the peptide backbone of Gly-863 and by an additional hydrogen bond of its oxygen atom to the side chain of Ser-904 (Fig. 4). We assume that PD128763 binds to PARP-CF in the same manner as the nicotinamide moiety of NAD^+. It binds much better than free nicotinamide, the IC_{50} value being by a factor of 200 lower (32). The fixed carbamoyl function of PD128763 and the nonpolar interactions with Tyr-907 may account for this difference. This observation agrees with a report stating that the carbamoyl orientation in nicotinamide analogue inhibitors is critical for PARP inhibition (33).

The carboxylate group of Glu-988, which has been shown to be important for catalytic activity (17), is at a distance of only 4 Å to the C^9 atom of PD128763 that is structurally equivalent to the anomeric $C1'_N$ atom of the nicotinamide ribose of NAD^+. At this location, Glu-988 could either function as a general base activating the second substrate for a nucleophilic attack an the $C1'_N$ atom of the bound NAD^+ (17) or by stabilizing an intermediate oxocarbenium ion at $C1'_N$ (21). This

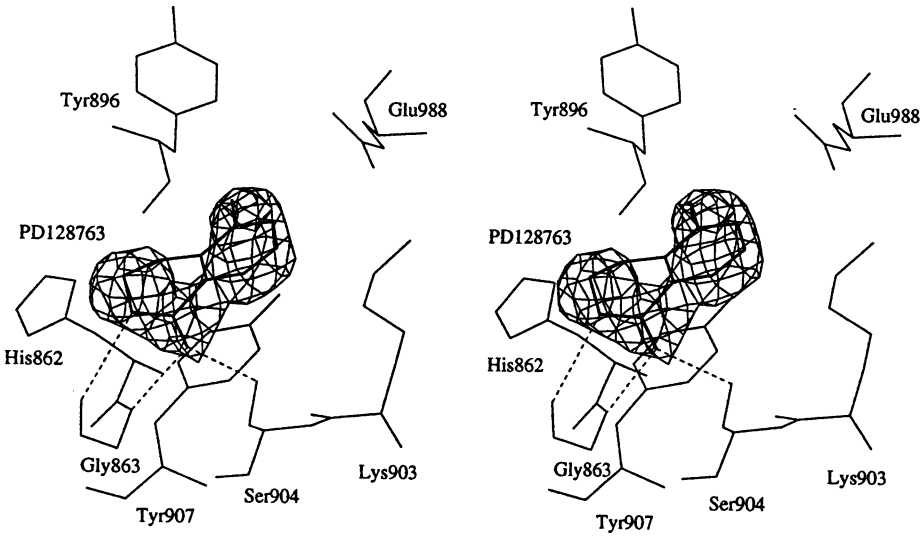

FIG. 4. Stereoview of the nicotinamide binding region of PARP-CF with the bound inhibitor PD128763. Hydrogen bonds are indicated by dashed lines. The initial ($F_o - F_c$) electron density is contoured at the 3σ level. At the 2σ level, all inhibitor atoms are in density.

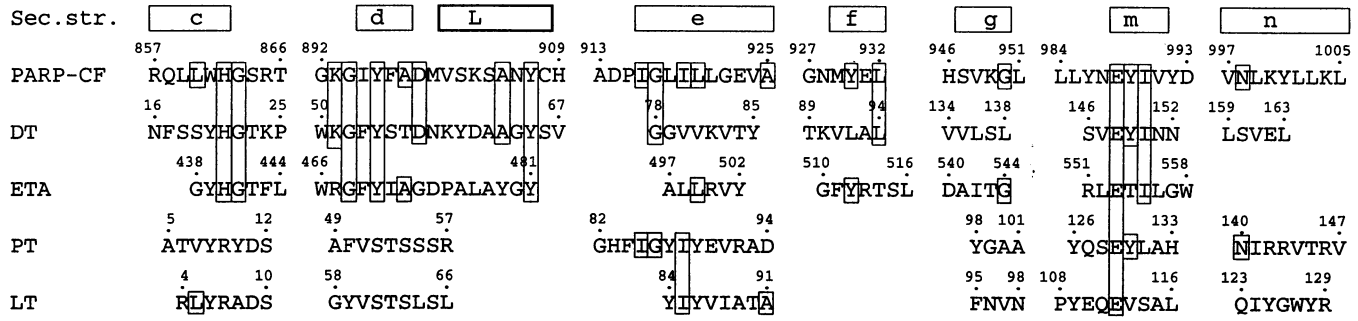

FIG. 5. Alignment of PARP-CF with bacterial toxins based on structural superpositions. The respective toxin residues are given as far as they deviate by less than 3.0 Å (cut-off) from their equivalents in PARP-CF. Conserved residues are boxed. See Fig. 2 for secondary structures. PARP-CF is given with human numbers; DT, dimeric diphtheria toxin; ETA, exotoxin A from *Pseudomonas aeruginosa* (23); PT, pertussis toxin (25); LT, heat-labile enterotoxin from *E. coli* (24). The superpositions of DT, ETA, PT, and LT with PARP-CF yield 59, 49, 50, and 44 aligned residues within the 3.0-Å cut-off, respectively. The corresponding rms C^{α} deviations were 1.4 Å, 1.3 Å, 1.5 Å, and 1.5 Å.

question is not decided by the virtually zero elongation and branching activities of mutants Glu-988 → Gln(Ala, Lys) (17, 34) because the replacements are neither general bases nor can they stabilize an oxocarbenium ion. It is also not decided by mutant Glu-988 → Asp showing moderately reduced elongation, branching, and initiation activities (17) because the displaced carboxylate explains the effect for both cases. Moreover, the merely moderately reduced initiation activities of mutants Glu-988 → Gln(Ala, Lys) provide no clue because initiation is generally started by a glutamate (from the regulating segment of PARP or from another protein) that needs no deprotonation and can also stabilize an oxocarbenium ion.

The Putative NAD^+ Binding Site. Given the inhibitor site (Fig. 4) and the observation that His-862 on β-strand c as well as Glu-988 on β-strand m are involved in NAD^+-binding or catalysis (17, 34), the adenosine site can be modeled. We suggest that NAD^+ binds in the cleft at the contact of the two central β-sheets, where it is lined by chain segment c-J-K-d-L as well as by segment m (Figs. 1 and 2). Segment c-J-K-d-L contains a block of 50 amino acids (residues 859–908) that are identical in all PARP sequences of vertebrates (6).

The NAD^+-binding chain fold motif is also present in all ADP-ribosylating toxins (35). Therefore, the NAD^+-binding site can also be deduced from the inhibitor adenylyl-3′,5′-uridine-3′-phosphate (ApUp) and from NAD^+ as bound to the catalytic domain of diphtheria toxin (19–21) or from AMP and nicotinamide as bound to *Pseudomonas* exotoxin A. A chain superposition based on the identical parts of the chain folds (Fig. 5) shows that the nicotinamide sites in exotoxin A (23) and diphtheria toxin (21) are in agreement with the PD128763 site in PARP-CF. Accordingly, the nicotinamide subsites are very similar in these three enzymes; moreover the involved residues Gly-863, Tyr-907, and Glu-988 are conserved (Fig. 5). In contrast, the environments of the adenosine subsites differ markedly. This site is shallow and solvent exposed in the bacterial toxins, whereas the putative adenosine site of PARP-CF is in a pocket lined by helix *F* of the additional N-terminal domain (Fig. 1*B*). We suggest that this N-terminal domain relays the signal of "PARP binding to nicked DNA" to the catalytic C-terminal domain by a relative rearrangement, giving rise to an NAD binding mode more favorable for catalysis.

A Superfamily of ADP-Ribosyl-Transferases. The superposition of ADP-ribosylating toxins and PARP-CF shows that the "inner" β-strands c, d, e, g, m, n of the central sheets as well as helix L are strongly conserved in all structures despite poor sequence similarity (Fig. 5). Moreover, the conserved active site glutamate (Glu-988 in PARP-CF) superimposes in all structures (Fig. 5). This striking similarity between eukaryotic PARP and prokaryotic toxins indicates that these enzymes are evolutionarily related. It is most unlikely that the rather complex topology of the NAD^+-binding fold (Fig. 2) has evolved independently. We therefore conclude that PARP-CF and the enzymatic fractions of the toxins constitute a superfamily of ADP-ribosyl-transferases with a common characteristic NAD^+-binding fold. This family is enlarged by mammalian mono(ADP-ribose) transferases as these show sequence- and thus certainly structural similarity with the ADP-ribosylating toxins (36).

We thank Sabine Jung and Everson Alves Miranda for their work at the early stages of the project, the team of the European Molecular Biology Laboratory outstation at Deutsches Elektronen Synchrotron (Hamburg) for help in data collection, and Parke–Davis/Warner–Lambert for the inhibitor PD128763. The project has been supported by the Deutsche Forschungsgemeinschaft under Contract SFB-388 (A.R. and G.E.S.), by the Association pour la Recherche Contre le Cancer and by La Ligue Nationale Contre le Cancer (G.M.d.M.).

1. Althaus, F. R. & Richter C. (1987) *Mol. Biol. Biochem. Biophys.* **37,** 1–126.
2. Lautier, D., Lagueux, J., Thibodeau, J., Ménard, L. & Poirier, G. G. (1993) *Mol. Cell. Biochem.* **122,** 171–193.
3. Molinete, M., Vermeulen, W., Bürkle, A., Ménissier de Murcia, J., Küpper, J., Hoeijmakers, J. & de Murcia, G. (1993) *EMBO J.* **12,** 2109–2117.
4. Satoh, M. S., Poirier, G. G. & Lindahl, T. (1993) *J. Biol. Chem.* **268,** 5480–5487.
5. Schreiber, V., Hunting, D., Trucco, C., Gowans, B., Grunwald, D., de Murcia, G. & Ménissier de Murcia, J. (1995) *Proc. Natl. Acad. Sci. USA* **92,** 4753–4757.
6. de Murcia, G. & Ménissier de Murcia, J. (1994) *Trends Biochem. Sci.* **19,** 172–176.
7. Simonin, F., Höfferer, L., Panzeter, P. L., Muller, S., de Murcia, G. & Althaus, F. R. (1993) *J. Biol. Chem.* **268,** 13454–13461.
8. Jung, S., Alves Miranda, E., Ménissier de Murcia, J., Niedergang, C., Delarue, M., Schulz, G. E. & de Murcia G. (1994) *J. Mol. Biol.* **244,** 114–116.
9. Otwinowski, Z. (1991) in *Isomorphous Replacement and Anomalous Scattering: Proceedings of the CCP4 Study Weekend 25–26 January 1991,* eds. Wolf W., Evans, P. R. & Leslie, A. G. W. (Science and Engineering Research Council, Daresbury Laboratory, Warrington, U.K.), Publ. DL/SCI/R32, pp. 80–85.
10. Cowtan, K. (1994) *Joint CCP4 and ESF-EACBM Newsl. Protein Crystallogr.* **31,** 34–38.
11. Jones, T. A., Zou, J.-Y., Cowan, S. W. & Kjeldgaard, M. (1991) *Acta Crystallogr. A* **47,** 110–119.
12. Brünger, A. T. (1992) X-PLOR Manual (Yale Univ. Press, New Haven, CT), Version 3.1.
13. Brünger, A. T. (1992) *Nature (London)* **355,** 472–475.
14. Laskowski, R. A., McArthur, M. W., Moss, D. S. & Thornton, J. M. (1993) *J. Appl. Crystallogr.* **26,** 283–291.
15. Domenighini, M., Montecucco, C., Ripka, W. C. & Rappuoli, R. (1991) *Mol. Microbiol.* **5,** 23–31.

16. Simonin, F., Poch, O., Delarue, M. & de Murcia, G. (1993) *J. Biol. Chem.* **268,** 8529–8535.
17. Marsischky, G. T., Wilson, B. A. & Collier, R. J. (1995) *J. Biol. Chem.* **270,** 3247–3255.
18. Choe, S., Bennett, M. J., Fujii, G., Curmi, P. M. G., Kantjardjieff, K. A., Collier, R. J. & Eisenberg, D. (1992) *Nature (London)* **357,** 216–222.
19. Bennett, M. J., Choe, S. & Eisenberg, D. (1994) *Protein Sci.* **3,** 1444–1463.
20. Weiss, M. S., Blanke, S. R., Collier, R. J. & Eisenberg, D. (1995) *Biochemistry* **34,** 773–781.
21. Bell, C. E. & Eisenberg, D. (1996) *Biochemistry* **35,** 1137–1149.
22. Allured, V. S., Collier, R. J., Carroll, S. F. & McKay, D. B. (1986) *Proc. Natl. Acad. Sci. USA* **83,** 1320–1324.
23. Li M., Dyda, F., Benhar, I., Pastan, I. & Davies, D. R. (1995) *Proc. Natl. Acad. Sci. USA* **92,** 9308–9312.
24. Sixma, T. K., Kalk, K. H., van Zanten, B. A. M., Dauter, Z., Kingma, J., Wiltholt, B. & Hol, W. G. H. (1993) *J. Mol. Biol.* **230,** 890–918.
25. Stein, P. E., Boodhoo, A., Armstrong, G. D., Cockle, S. A., Klein, M. H. & Read, R. J. (1994) *Structure* **2,** 45–57.
26. Zhang, R.-G., Scott, D. L., Westbrook, M. L., Nance, S., Spangler, B. D., Shipley, G. G. & Westbrook, E. M. (1995) *J. Mol. Biol.* **251,** 563–573.
27. Baker, P. J., Britton, K. L., Engel, P. C., Farrants, G. W., Lilley, K. S., Rice, D. W. & Stillman, T. J. (1992) *Proteins* **12,** 75–86.
28. Ben-Hur, E., Utsumi, H. & Elkind, M. M. (1984) *Radiat. Res.* **97,** 546–555.
29. Arundel-Suto, C. M., Scavone, S. V., Turner, W. R., Suto, M. J. & Sebolt-Leopold, J. S. (1991) *Radiat. Res.* **126,** 367–371.
30. Sebolt-Leopold, J. S. & Scavone, S. V. (1992) *Int. J. Radiat. Oncol. Biol. Phys.* **22,** 619–621.
31. Suto, M. J., Turner, W. R., Werbel, L. M., Arundel-Suto, C. M. & Sebolt-Leopold, J. S. (1991) *Anticancer Drug Des.* **7,** 107–117.
32. Suto, M. J. & Suto, C. M. (1991) *Drugs Future* **16,** 723–739.
33. Griffin, R. J., Curtin, N. J., Newell, D. R., Golding, B. T., Durkacz, B. W. & Calvert, A. H. (1995) *Biochimie* **77,** 408–422.
34. Masson, M., Rolli, V., Dantzer, F., Trucco, C., Schreiber, V., Fribourg, S., Molinete, M., Ruf, A., Alves Miranda, E., Niedergang, C., Hunting, D., Gowans, B., Schulz, G. E., Ménissier de Murcia, J. & de Murcia, G. (1995) *Biochimie* **77,** 456–461.
35. Domenighini, M., Magagnoli, C., Pizza, M. & Rappuoli, R. (1994) *Mol. Microbiol.* **14,** 41–50.
36. Okazaki, I. J. & Moss, J. (1994) *Mol. Cell. Biochem.* **138,** 177–181.